

**RELAP5/MOD3.2 Analysis of INSC Standard Problem INSCSP-R7:
Void Fraction Distribution over RBMK Fuel Channel Height for Experiments
Performed in the ENTEK BM Test Facility**

Patrick L. Garner, Argonne National Laboratory
9700 South Cass Avenue, Argonne, Illinois 60439 USA
(1-630) 252-4872, PLGarner@anl.gov

Abstract

The RELAP5/MOD3.2 computer program has been used to analyze a series of tests investigating void fraction distribution over height in RBMK fuel channels performed in Facility BM at the ENTEK. This is RBMK Standard Problem 7 in Joint Project 6, which is the investigation of Computer Code Validation for Transient Analysis of RBMK and VVER Reactors, between the United States and Russian Minatom International Nuclear Safety Centers. The experiment facility and data, RELAP5 nodalization, and results are shown for all tests. Agreement between RELAP5 and the experiment data is reasonable.

1. Introduction

RBMK reactors were designed in the 1970s, before the current Russian licensing requirements were issued. Hence, the Safety Analysis Reports (SAR) for these reactors do not completely satisfy current requirements. These reactors continue to operate in Russia and Lithuania, generating a significant share of the total energy source

in these countries. Since these reactors are expected to continue operating for many more years, up-to-date SARs are being established which require verification and use of best-estimate codes like RELAP5.

The RBMK design and operating conditions (e.g., channelized flow with boiling coolant) are distinctly different from other reactor types in the world; therefore, it is not possible to use worldwide experience and data to the extent that is possible for the VVER type reactors (which have many similarities to the pressurized water reactors used in many countries). There are Russian experiment data applicable to RBMK reactors, although most of these experiments were performed in the 1970s and 1980s and are not fully suitable for current-day code validation activities. RELAP5 validation for RBMK reactors is an important issue but is a more difficult task compared with validation for VVER reactors.

A joint US/Russian project has been established to address RELAP5 validation issues for both RBMK and VVER reactors. The technical work involves participation by staff from many US and Russian organizations. The work is coordinated by each country's International Nuclear Safety Center (i.e., USINSC in the US and

RMINSK in Russia under Minatom). The work is funded by the United States Department of Energy (USDOE) through its International Nuclear Safety Program (INSP). Work has proceeded in parallel for both RBMK and VVER reactors; only the RBMK work is mentioned here. Phase 1 of this project (Reference 1) was the identification of the phenomena expected to be important in RBMK safety analysis, identification of experiment facilities and data relevant to these phenomena, prioritizing the phenomena on the basis of their importance to the safety analysis process, and categorizing the experiment data as to their relevance to the validation process. A set of guidelines (Reference 2) was prepared during Phase 1 describing how Standard Problems (SP) would be defined and analyzed. During Phase 1, one set of RBMK experiment data was analyzed by both Russian and US teams using RELAP5 as an example of the process to be followed in subsequent SPs: i.e., preparation of a data report by the data owner, analysis and its reporting by each team, preparation of a joint analysis report summarizing the results from all teams, and storing all of the information in such a manner that it is accessible via the internet. During Phase 2, the list of potential Standard Problems was reduced to those having a high impact on safety and for which experiment data were both available and suitable for analysis using RELAP5; the list was then prioritized (Reference 3) resulting in a set of 12 SPs for RBMK; Phase 2 also showed there are some phenomena for which there are insufficient Russian experiment data to define SPs for analysis. Phase 3 of the project is the analysis of the first six SPs for each of these two reactor designs. (Much of the preceding three paragraphs was extracted from Reference 4.)

The present report is the US analysis of INSC Standard Problem RBMK Number 7 (INSC SP-R7). This is the fourth RBMK SP to be analyzed chronologically (INSC SP-R1 was analyzed during Phase 1, and R5 and R2 were analyzed previously in Phase 3), even though its "R7" identifier would indicate the seventh problem. Identifiers (i.e., R1-R12) were assigned to the SPs during Phase 2, and the numeric part of the identifier indicates the analysis order based on the prioritization process; since that time, data availabilities have required the problems to be analyzed in a different order than originally planned.

Sections 2 and 3 of this report describe the experiment facility and the tests, respectively, which examine the axial distribution of coolant void in an RBMK coolant channel at steady state. Sections 4 through 6 present the results of applying RELAP5 to these experiment conditions. Conclusions from this analysis are shown in Section 7. A similar report is being prepared by the Russian analysis team. These two reports will be used to prepare a comparative analysis report covering the work of both teams.

2. Description of Facility BM

The BM Facility at the Research and Development Institute of Power Engineering (RDIPE; a.k.a., ENTEK and NIKIET) models the forced circulation circuit of RBMK type reactors (Reference 5). The facility includes simulated fuel channels (two), steam separator, condenser, pump, and connecting piping; there are several different flow configurations. For the void distribution tests being studied, only a single fuel channel was used and the facility was at steady state. Several views of the facility

relevant to the current experiments are shown in Figures 2.1 through 2.2.

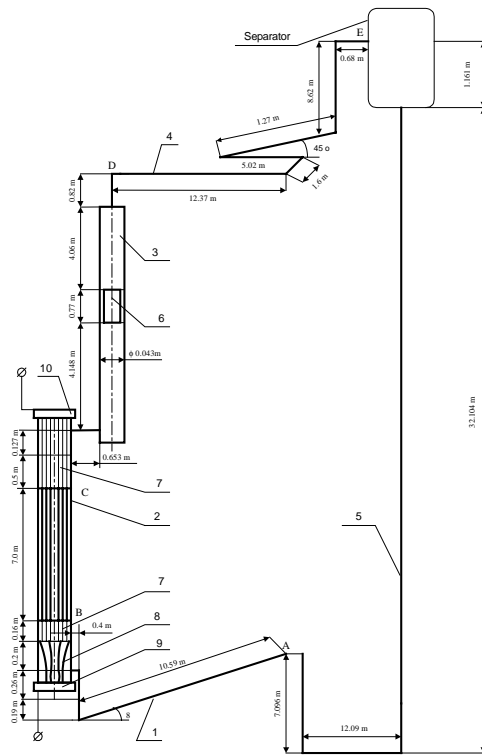


Fig. 2.1 Overall Schematic of BM Facility

Figure 2.1 provides an overall flow diagram of the single loop, showing component lengths. Coolant flow enters the simulated flow channel horizontally in the region labeled “8”, travels upward through the Heat Release Zone (HRZ; i.e., fuel rod simulators) between points “B” and “C”, and exits horizontally just below the upper flange labeled “10”.

Figure 2.2 provides a cross-section view of the HRZ, where diameters are shown in millimeters. The HRZ contains a 7-rod bundle; the stainless steel (X18H10T) rods are hollow, having an outer diameter of 13.5 mm, a 1.25 mm wall thickness, and a 7 m length. The bundle is contained within a stainless steel pressure tube (80 mm outer diameter and 5 mm wall thickness), which is lined with a set of talcum chlorate thimbles

(49 mm inner diameter and 10.5 mm wall thickness). The coolant flow area is $8.84 \times 10^{-4} \text{ m}^2$ and the hydraulic diameter is 7.84 mm. Copper tips (“7” in Figure 2.1) are welded to the end of the fuel pin simulators to supply current; these are connected to the supply flanges (“9” and “10” in Figure 2.1) by flexible conductors (“8” in Figure 2.1). Electrical heating is stated to be uniform over rod height and over fuel assembly radius. There are 20 honeycomb-type pin spacing grids along the length of the HRZ, starting 30 mm from the beginning of the HRZ and repeated every 350 mm; these are similar to the spacers in the RBMK-1000 and have a hydraulic loss coefficient of 0.4 based on measurements.

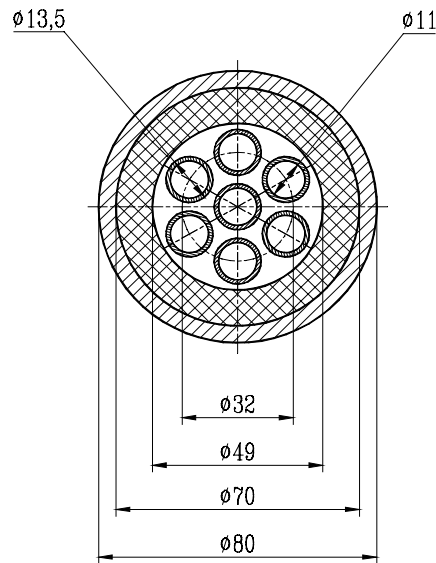


Fig. 2.2 Cross-Section of Heat Release Zone
(ϕ is diameter in mm.)

The test section was surrounded by an asbestos overcoat. The thickness and properties of this overcoat were not specified. The intent was to keep the exterior surface temperature below 313 K. Heat loss from the facility was measured during a series of constant-temperature experiments. The loss from the heat-release

zone was 4.5 kW at 436 K, 6.9 kW at 475 K, 9 kW at 515 K, and 11.2 kW at 535 K.

The specifics of the rest of the facility are not important for the current set of experiments.

Properties of X18H10T stainless steel were given as follows: density (ρ) of 6400 kg/m³ and specific heat capacity (C_p) of 490 J/kg•K as constant from 300 to 2000 K, and thermal conductivity (ν) values of 15.0, 17.0, 19.8, 26.6, 27.8, and 29.4 W/m•K at 300, 400, 600, 1000, 1500, and 2000 K. Properties of talcum chlorate were given as follows: density of 2790 kg/m³, specific heat capacity of 460 J/kg•K, and thermal conductivity of 1 W/m•K.

The following measurements (and associated accuracies) were made during each test

- pressure at HRZ outlet, point “C” of Figure 2.1 ($\pm 1.5\%$);
- coolant mass flow rate (± 2.08 kg/s•m² which translates to ± 0.0018 kg/s);
- coolant temperature at HRZ inlet, point “B” of Figure 2.1 (± 1 K);
- electrical power (± 947 W/m² which translates to ± 2 kW);
- coolant density (± 8 kg/m³ at 10 axial levels);
- coolant density sensor location (± 2 mm); and
- void fraction (± 0.03 ; void is calculated rather than measured).

The location of the pressure and temperature measurements (among other things) allows the RELAP5 modeling to only include the HRZ, i.e., points “B” through “C” of Figure 2.1.

Coolant density was detected based on the coolant’s attenuation of neutrons from a Pu-Be source as measured external to the HRZ.

There was only one source/sensor combination. Readings were obtained at 10 axial locations (i.e., 0.385, 0.948, 1.573, 2.322, 2.947, 4.010, 4.823, 5.448, 6.135, and 6.760 m from bottom of heated length) by moving the equipment during a test. For some tests, the boundary conditions shifted somewhat during the time required to obtain measurements at all ten locations; these shifts were recorded. The direct measurement is counts/s. This was converted to a mixture density (ρ_m) based on attenuation rules, and the result was reported in Reference 5. The density was converted to a void fraction (ν) using

$$\nu = (\rho_l - \rho_m) / (\rho_l - \rho_v)$$

and the value was reported in Reference 5. In this expression, ρ_l is the liquid phase coolant density at the measured (i.e., outlet) pressure and local coolant temperature calculated based on heating the coolant over the non-boiling length. The quantity ρ_v is the steam phase density at saturation for the test’s pressure. Void fraction is reported as “0” if the above procedure results in a negative value.

3. Description of Tests

Data were obtained from the facility at steady state for 25 combinations of outlet pressure (i.e., 3 and 7 MPa), coolant flow rate (i.e., 0.4 to 1.8 kg/s), inlet temperature (i.e., 329 to 540 K), and heater power (i.e., 290 to 630 kW). For each of these combinations, coolant density readings were made at each of the 10 axial levels (sequentially). Since the coolant density had to be measured at each of the locations sequentially rather than simultaneously, the four global boundary conditions (i.e., pressure, flow rate, temperature, and power) were recorded during each of the ten density measurements in order to report any changes within a test sequence.

4. RELAP5/MOD3.2 Modeling

Although Facility BM has a closed coolant flow loop, the tests were run in a mode such that the inlet temperature and exit pressure were constant (and known) during a data measurement sequence. Therefore, the analysis with RELAP5/MOD3.2 (Reference 6) modeled only the heat release zone (i.e., between points “B” and “C” in Figure 2.1). The nodalization used in the RELAP5 model is shown in Figure 4.1.

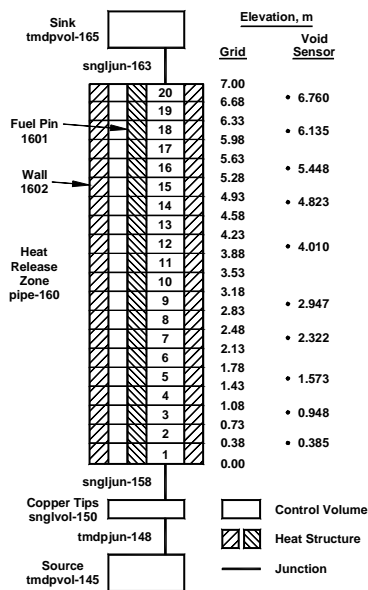


Fig. 4.1 RELAP5 Nodalization for HRZ

The heat release zone is represented by pipe component 160. This RELAP component is divided into 20 volumes. The lowest volume has a length of 0.38 m, the highest volume has a length of 0.32 m, and the other volumes have a length of 0.35 m each. This axial noding choice places the 19 interior junctions at locations of 19 of the spacer grids. The 20th spacer grid is physically located 0.03 m above the lower end of the heat release zone; in the RELAP model, it is

located at the bottom of the heat release zone, being represented by a hydraulic loss in junction 158. The hydraulic loss factor was 0.4 for each spacer grid. The flow area ($8.84 \times 10^{-4} \text{ m}^2$) and hydraulic diameter (7.84 mm) for this region were as given in the Definition report.

Each of the seven heater rods is modeled as hollow cylinder heat structure 1601, having a 13.5 mm outer diameter and a 11 mm inner diameter. The axial noding was identical to that in fluid component 160. The steel annulus was divided into two intervals. The heat source was distributed uniformly, both within a rod radially and axially and from rod to rod. The total power from all rods (N) was input from the experiment conditions using general table 001; this was converted to a per rod power in control variable 001. Heat transfer from the outer surface of the rods to the coolant in component 160 was via convection using convection type 110 (vertical bundle without crossflow). The inner surface of the rods was adiabatic.

The outer wall of the test section was modeled as a two-region cylinder. The inner cylinder has an inner diameter of 49 mm, a thickness of 10.5 mm, and is composed of talcum chlorate; it was modeled using 3 intervals of equal thickness. The outer cylinder is steel and has a thickness of 5 mm; it was modeled using 2 intervals of equal thickness. The inner surface of the cylinder exchanges heat with the fluid in component 160 via convection of type 1. Rather than model the asbestos overcoat (of unknown thickness and material properties), the outer surface was treated adiabatic and the heat loss was modeled as a negative heat source in the outermost steel interval; the heat loss at axial node n is supplied from control variable 40+n, which uses the liquid temperature in volume n of component 160

in the heat-loss table defined by general table 002 (using the 4 points given in Section 2 plus assuming zero heat loss at 293 K) to obtain the total heat loss, multiplied by the fractional height of axial node n compared to the 7-m total length.

The 0.16-m region containing the copper tips supplying current to the bottom of the heater rods was modeled as single volume component 150, having the same flow area and hydraulic diameter as the heated zone. This region was modeled in order for there to be a single junction, 158, at the bottom of component 160 in which to model the loss associated with the lowest spacer grid.

The coolant source is represented by time-dependent volume 145, for which temperature and pressure are specified. The temperature comes directly from the experiment data (T_{in}). The inlet pressure was estimated to be somewhat larger than the exit pressure for input to initial calculation runs; later calculation runs used the value calculated from volume 150 in a previous run. The calculated results were not sensitive to the initial pressure specified in volume 145.

Volumes 145 and 150 are separated by time-dependent junction 148. The mass flow rate through this junction is specified to match the mass flow rate (G) in the experiment.

Time dependent volume 165 provides a pressure boundary condition on the system with the value (P_{ex}) coming from the experiment data. This volume connects to the outlet of component 160 through single junction 163.

As shown in Figure 4.1, the calculation model does not align perfectly with the 10 measurement locations for density. The noding was chosen so that the junctions

between volumes align with the spacer grids, rather than aligning volume centers with the void sensor positions. In order to facilitate comparison of calculated results to measured results, a set of control variables were defined in RELAP to compute values at the sensor locations by linearly interpolating from the volume average values computed by RELAP. For example, the lowest density sensor is located 0.385 m above the bottom of the heated section; this is just above the junction separating the lowest two volumes in component 160; therefore, assuming that the RELAP values are associated with the volume centers, the density at the sensor location is computed using

$$\rho_{0.385} = [\rho_{0.19} * (0.555-0.385) + \rho_{0.555} * (0.385-0.19)] / (0.555-0.19),$$

where 0.19 and 0.555 m are the elevations of the centers of volumes 1 and 2 of component 160 and $\rho_{0.19}$ and $\rho_{0.555}$ are the mixture densities printed by RELAP for these two volumes. Control variables for void fraction (cntrlvar 020 – 029) and quality (100 – 109) at the sensor locations were defined in a manner similar to those for density (110 – 119).

A preliminary RELAP calculation was performed for each of the 25 experiments in order to obtain an estimate of the inlet pressure to be used in the subsequent calculations. Next, a base RELAP calculation (denoted “Calc42”) was performed for each of the 25 experiments which used the average pressure, mass flow rate, power, and inlet temperature for the 10 experiment runs needed to obtain the measurements at the 10 axial positions. Several additional RELAP calculations were performed as described in Section 6.

Each RELAP case was started in steady-state mode (i.e., entering “stdy-st” on Card

100). For most of the experiments, the RELAP code would declare steady state had been achieved after 30 to 40 s of case time. A review of the results at this time typically showed that the heat structures had not achieved thermal equilibrium. Therefore, the case was then continued in transient mode (i.e., entering “transnt” on Card 100) for another 50-60 s, by which time equilibrium had been achieved. This combination of steady-state and transient cases required less computer time than running the entire case in transient mode.

5. Results

The standard problem definition (Reference 5) states a preference for void fraction as the primary quantity to be compared between calculation and experiment. The experiment conditions are shown along with the experiment and calculation results for void fraction in Table 5.1. Within a test series, there is one row of entries for each of the ten axial levels (“Z”). The “Exp”, “Calc” and “v” columns are the experiment results, the calculated results, and the difference between calculated and experiment results. The header row of information for each test series shows the average of the boundary conditions for the series of 10 measurements.

As shown in Table 5.1, the calculated results for void fraction follow the same trend with axial position as the experiment results. Most (i.e., 70%) of the calculated values are within the ± 0.03 experiment error margin of the experiment results. This can be classed as “reasonable” agreement in the style of the qualitative standard in the Project 6 Guideline (Reference 2).

For the void fraction values outside of the ± 0.03 accuracy limit, the void fraction

calculated by RELAP is more likely (i.e., in approximately 75% of these measurements) to be lower than the experiment void than higher. The percentage of cases where the void fraction is low is higher for the high pressure cases than for the low pressure cases. Otherwise, there is no identifiable trend between level of error (i.e., between calculation and experiment) and the experiment boundary conditions.

Of the 10 points in each test, the one most likely to show a discrepancy between the calculation and the experiment is the lowest elevation point having a positive void fraction. This is a direct consequence of the somewhat coarse noding (i.e., 20 axial nodes covering 7 m) in the calculation model. There was no attempt to improve this by using smaller height nodes. One probably would not be able to use smaller nodes in a calculation for a power plant having multiple channels.

Although not shown here, the results trends and errors for density and quality are similar to those seen for void fraction. There are a couple of interesting observations. Density is somewhat harder than void fraction to match at low elevations; the calculation and the experiment are more likely to agree within ± 0.03 about a void fraction of 0.0 than to agree within $\pm 8 \text{ kg/m}^3$ about a density of 800 kg/m^3 .

6. Sensitivity Assessment

One approach (denoted “Calc47”) to investigating the experiment variations on results would be to perform RELAP calculations using the specific pressure, mass flow rate, power, and inlet temperature as measured in each of the 10 measurement sequences for each test. Instead, the present work has attempted to bound the result by

performing only 2 extra RELAP calculations per test: one which minimized the void and one which maximized the void. The minimum void case used the maximum pressure, the maximum mass flow rate, the minimum inlet temperature, and the minimum power of the 10 measurement sequences for each test; the set of results for minimum void is shown as “Calc43” in the figures. The maximum void case used the minimum pressure, the minimum mass flow rate, the maximum inlet temperature, and the maximum power of the 10 measurement sequences for each test; the set of results for maximum void is shown as “Calc44” in the figures. The calculation points which form “Calc43” and “Calc44” are connected with dashed lines in the figures in order to illustrate the bounding effect, although connection of the points with such a line is probably not appropriate due to the discreteness of the data. Note that the spread in boundary conditions from minimum void to maximum void may be larger than the stated experiment error. There are only 10% of experiment void fraction points for which some part of the range of the experiment measurement for void fraction plus or minus its experiment error range is not within these minimum and maximum void calculations.

The comparison of results is shown graphically for Regimes 20, 7, and 19 in Figures 5.1 through 5.3, respectively. These figures illustrate somewhat different behaviors.

For Regime 20 in Figure 5.1, the base calculated results (i.e., Calc42) are very similar to the experiment results. The calculation is significantly low at 4.8 m, although the experiment data looks higher than would be expected for normal trending. There is only a small difference between the results calculated using boundary conditions

which favor minimum voiding (i.e., Calc43) and those which favor maximum voiding (i.e., Calc44); this indicates that the boundary conditions were, indeed, reasonably stable during the Regime 20 tests.

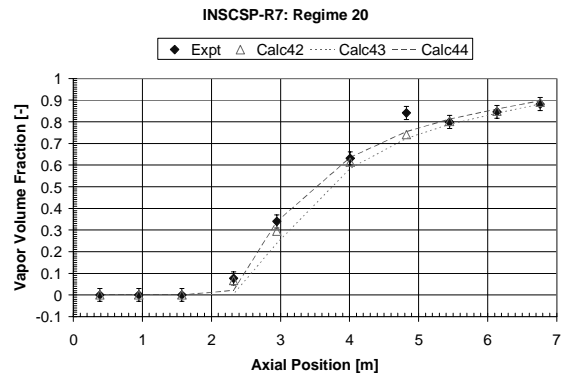


Fig. 5.1 Void versus Position for Regime 20

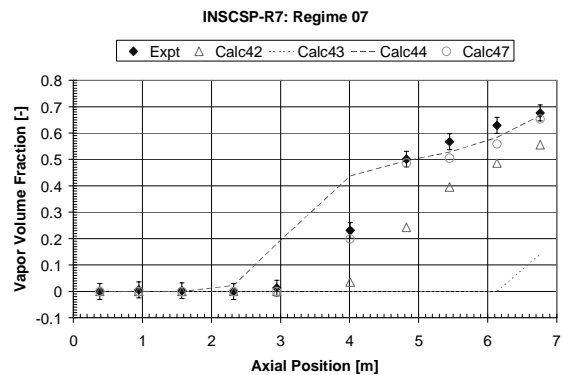


Fig. 5.2 Void versus Position for Regime 7

For Regime 7 in Figure 5.2, the base calculation is too low for all the non-zero points. The results calculated using boundary conditions which favor minimum and maximum voiding span a very wide range; this indicates that there were significant changes in boundary conditions during the Regime 7 tests. Based on a sensitivity calculation shown as “Calc47” in Figure 5.2, the calculation is greatly improved if the actual boundary conditions for each axial level are used rather than using one set of average boundary conditions for all 10 axial levels. The use of average boundary conditions was a poor

approximation here due to the variations in boundary conditions, especially the 21 K variation in inlet temperature.

For Regime 19 in Figure 5.3, the base calculations are significantly below the experiment results. The spread between minimum and maximum void boundary conditions is moderately wide but not wide enough to encompass the experiment data. Regimes 19 and 7 have the same mass flow rate, same heat source, and same inlet subcooling; the two regimes differ in pressure. The differences in behavior between Regime 19 and Regime 7 are not understood.

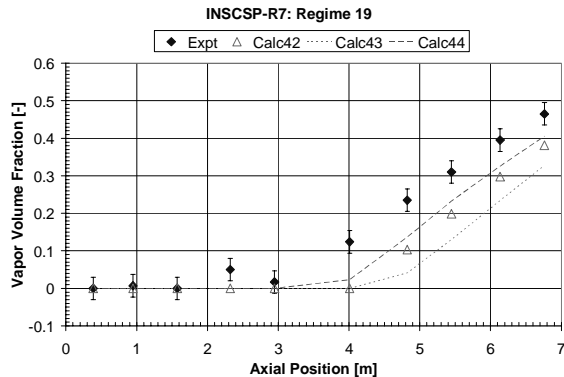


Fig. 5.3 Void versus Position for Regime 19

Four potential error sources are as follows. There was concern about using the exit pressure instead of the local pressure in the formula which converted measured density to void fraction; a sample calculation for the conditions of test 03 showed that the shift from exit to inlet pressure made no significant change (i.e., <0.001) in the calculated void fraction. The coarseness of the axial mesh limits the accuracy with which void fraction can be calculated; the cell-average value from RELAP5 is being compared with a point-wise measurement from the experiment; this will be most noticeable at the lowest axial location having a positive void fraction. Radial temperature variations could allow voiding to occur in a radially limited portion of the

HRZ cross section in the experiment; this was probably not detectable with the density measuring device (and, if measured, was not reported). Variation in electrical resistivity with temperature could result in heat generation being non-uniform axially instead of the assumed (and stated) uniformity. These last three error sources were not investigated computationally.

7. Conclusions

The RELAP5/MOD3.2 computer program has been used to analyze experiments performed in ENTEK Facility BM which investigated axial coolant void distribution in an RBMK flow channel at steady state. All 25 tests were analyzed. Most (70%) of the calculated results for void fraction are within the ± 0.03 accuracy margin of the experiment results. This is considered “reasonable” agreement.

References

1. “Validation Prioritization on RBMK” (Deliverable 6 of Task 2 of Phase 1 of Joint Project 6 with the United States International Nuclear Safety Center), International Nuclear Safety Center of Russia Minatom (January 1998).
2. “Guideline for Performing Code Validation within the DOE International Nuclear Safety Center (Deliverable 4 of Task 2 of Phase 1 of Joint Project 6 with the International Nuclear Safety Center), International Nuclear Safety Center of Russia Minatom (September 1997).
3. G. I. Savvatimski, A. Ya. Kramerov, L. L. Kobzar, V. A. Vinogradov, Yu. V. Mironov, V. N. Smolin, V. N. Blinkov, N. A. Brus, O. Ioussouпов, J. Roglans, P.

Garner, and B. Schmitt, “Final RELAP5 Validation Plan for Application to RBMK (Deliverable b of Task 3 of Phase 2 of Joint Project 6 with the United States International Nuclear Safety Center) , International Nuclear Safety Center of Russia Minatom (June 1998).

4. Bruce E. Schmitt, “RELAP5 Analysis of INSC Standard Problem R1: KS Facility Experiments on Coolant Flow Stop under Decay Heat Removal on FC RBMK Model Conducted in Russian Research Center Kurchatov Institute” (draft), Pacific Northwest National Laboratory, Richland, Washington (October 1998).

5. N. A. Brus and O. E. Ioussoupov, “Experimental Data on INSC SP-R7 Standard Problem for RBMK: Void Fraction Distribution over RBMK FC Height – Experiments Performed on the ENTEK BM Test Facility” (Deliverable R7-1 of Work Order 5 of Phase 3 of Joint Project 6 with the United States International Nuclear Safety Center), International Nuclear Safety Center of Russia Minatom (July 2000).

6. The RELAP5 Code Development Team, “RELAP5/MOD3 Code Manual”, NUREG/CR-5535 (INEL-95/0174), Volumes I-V, Idaho National Engineering Laboratory, Idaho Falls, Idaho (June 1995).

The submitted manuscript has been created by the University of Chicago as Operator of Argonne National Laboratory (“Argonne”) under Contract No. W-31-109-ENG-38 with the U.S. Department of Energy. The U.S. Government retains for itself, and others acting on its behalf, a paid-up, nonexclusive, irrevocable worldwide license in said article to reproduce, prepare derivative works, distribute copies to the public, and perform publicly and display publicly, by or on behalf of the Government.

R7_pap1.doc
August 8, 2002

NOTICES

Argonne National Laboratory’s work was supported by the U. S. Department of Energy, National Nuclear Security Administration, Assistant Deputy Administrator for International Nuclear Safety and Cooperation, under contract W-31-109-Eng-38.

Table 4.1 Void Fraction Results

Z, m	v		
	Exp	Calc	Δ
Reg. 1: P=3.1, N=300, G=0.44, T=387			
0.385	0	0	0
0.948	0	0	0
1.573	0	0	0
2.322	0	0	0
2.947	0	0	0
4.01	0	0	0
4.823	0.027	0	-0.027
5.448	0.178	0.175	-0.003
6.135	0.493	0.509	0.016
6.76	0.635	0.622	-0.013
Reg. 2: P=3.1, N=299, G=0.44, T=482			
0.385	0.002	0	-0.002
0.948	0.122	0.023	-0.099
1.573	0.368	0.371	0.003
2.322	0.592	0.606	0.014
2.947	0.668	0.647	-0.021
4.01	0.734	0.755	0.021
4.823	0.792	0.805	0.013
5.448	0.804	0.834	0.030
6.135	0.819	0.860	0.041
6.76	0.85	0.888	0.038
Reg. 3: P=3.1, N=299, G=0.44, T=487			
0.385	0	0	0
0.948	0.218	0.155	-0.063
1.573	0.439	0.473	0.034
2.322	0.592	0.589	-0.003
2.947	0.675	0.679	0.004
4.01	0.737	0.772	0.035
4.823	0.779	0.817	0.038
5.448	0.803	0.844	0.041
6.135	0.82	0.868	0.048
6.76	0.845	0.894	0.049
Reg. 4: P=3.1, N=298, G=0.88, T=451			
0.385	0	0	0
0.948	0.006	0	-0.006
1.573	0.015	0	-0.015
2.322	0	0	0
2.947	0.002	0	-0.002
4.01	0.002	0	-0.002
4.823	0.043	0.009	-0.034
5.448	0.136	0.164	0.028
6.145	0.299	0.415	0.116
6.76	0.472	0.525	0.053

	v		
	Exp	Calc	Δ
Reg. 5: P=3.1, N=295, G=0.87, T=484			
0.948	0.003	0	-0.003
1.573	0.053	0	-0.053
2.322	0.174	0.125	-0.049
2.947	0.335	0.366	0.031
4.01	0.549	0.511	-0.038
4.823	0.62	0.603	-0.017
5.448	0.667	0.657	-0.010
6.135	0.708	0.702	-0.006
6.76	0.76	0.758	-0.002
Reg. 6: P=3.1, N=296, G=1.31, T=486			
0.385	0	0	0
0.948	0.009	0	-0.009
1.573	0.009	0	-0.009
2.322	0	0	0
2.947	0.097	0.019	-0.078
4.01	0.32	0.323	0.003
4.823	0.459	0.482	0.023
5.448	0.552	0.499	-0.053
6.135	0.604	0.562	-0.042
6.76	0.667	0.647	-0.020
Reg. 7: P=3.1, N=305, G=1.76, T=486			
0.385	0	0	0
0.948	0.006	0	-0.006
1.573	0.003	0	-0.003
2.322	0	0	0
2.822	0.013	0	-0.013
4.01	0.231	0.035	-0.196
4.823	0.501	0.243	-0.258
5.448	0.567	0.396	-0.171
6.135	0.629	0.486	-0.143
6.76	0.676	0.555	-0.121
Reg. 8: P=3.1, N=524, G=0.45, T=341			
0.385	0.003	0	-0.003
0.948	0.01	0	-0.010
1.573	0.001	0	-0.001
2.322	0	0	0
2.947	0	0	0
4.01	0.206	0.058	-0.148
4.823	0.621	0.570	-0.051
5.448	0.756	0.691	-0.065
6.135	0.83	0.788	-0.042
6.76	0.86	0.850	-0.010
Reg. 9: P=3.1, N=525, G=0.44, T=455			
0.385	0.022	0	-0.022
0.948	0.121	0.019	-0.102
1.573	0.5	0.419	-0.081

Z, m	v		
	Exp	Calc	Δ
2.322	0.692	0.650	-0.042
2.947	0.783	0.758	-0.025
4.01	0.831	0.853	0.022
4.823	0.859	0.897	0.038
5.448	0.889	0.923	0.034
6.135	0.91	0.958	0.048
6.76	0.965	0.973	0.008
Reg. 10: P=3.1, N=504, G=0.88, T=427			
0.385	0	0	0
1.198	0.001	0	-0.001
1.573	0.006	0	-0.006
2.322	0	0	0
2.947	0.006	0	-0.006
4.01	0.165	0.031	-0.134
4.823	0.398	0.405	0.007
5.448	0.541	0.518	-0.023
6.135	0.652	0.638	-0.014
6.76	0.74	0.732	-0.008
Reg. 11: P=3.1, N=504, G=0.88, T=486			
0.385	0.001	0	-0.001
0.948	0.106	0.030	-0.076
1.573	0.315	0.338	0.023
2.322	0.5	0.507	0.007
2.947	0.64	0.621	-0.019
4.01	0.724	0.736	0.012
4.823	0.773	0.794	0.021
5.448	0.803	0.831	0.028
6.135	0.828	0.889	0.061
6.76	0.858	0.923	0.065
Reg. 12: P=3.1, N=504, G=1.33, T=449			
0.385	0	0	0
0.948	0.007	0	-0.007
1.573	0.004	0	-0.004
2.322	0	0	0
2.947	0	0	0
4.01	0.044	0	-0.044
4.823	0.254	0.118	-0.136
5.448	0.382	0.390	0.008
6.135	0.521	0.497	-0.024
6.76	0.645	0.614	-0.030
Reg. 13: P=3.1, N=501, G=1.33, T=488			
0.385	0.005	0	-0.005
0.948	0.022	0	-0.022
1.573	0.206	0.026	-0.180
2.322	0.337	0.319	-0.018
2.947	0.486	0.481	-0.005
4.01	0.634	0.598	-0.036

	v		
	Exp	Calc	Δ
4.823	0.696	0.680	-0.016
5.448	0.731	0.729	-0.002
6.135	0.752	0.782	0.030
6.76	0.785	0.853	0.068
Reg. 14: P=3.1, N=511, G=1.76, T=476			
0.385	0.002	0	-0.002
0.948	0.001	0	-0.001
1.573	0	0	0
2.322	0	0	0
2.947	0	0	0
4.01	0.24	0.235	-0.005
4.823	0.484	0.476	-0.008
5.448	0.594	0.514	-0.080
6.135	0.646	0.597	-0.049
6.76	0.718	0.694	-0.024
Reg. 15: P=7.2, N=304, G=0.44, T=439			
0.385	0	0	0
0.948	0.008	0	-0.008
1.573	0.01	0	-0.010
2.322	0	0	0
2.947	0.003	0	-0.003
4.01	0	0	0
4.823	0.017	0	-0.017
5.448	0.087	0	-0.087
6.135	0.253	0.236	-0.018
6.76	0.438	0.427	-0.011
Reg. 16: P=7.2, N=304, G=0.44, T=512			
0.385	0	0	0
0.948	0.003	0	-0.003
1.573	0.017	0	-0.017
2.322	0.164	0.100	-0.064
2.947	0.363	0.317	-0.046
4.01	0.577	0.528	-0.049
4.823	0.67	0.633	-0.037
5.448	0.723	0.694	-0.029
6.135	0.783	0.744	-0.039
6.76	0.796	0.792	-0.004
Reg. 17: P=7.2, N=303, G=0.88, T=496			
0.385	0	0	0
0.948	0.004	0	-0.004
1.573	0.006	0	-0.006
2.322	0	0	0
2.947	0.009	0	-0.009
4.01	0.002	0	-0.002
4.823	0.017	0	-0.017
5.448	0.033	0	-0.033
6.135	0.079	0.028	-0.051

Z, m	v		
	Exp	Calc	Δ
6.76	0.194	0.162	-0.032
Reg. 18: P=7.1, N=303, G=0.88, T=525			
0.385	0	0	0
0.948	0.003	0	-0.003
1.573	0	0	0
2.322	0.009	0	-0.009
2.947	0.089	0	-0.089
4.01	0.275	0.189	-0.086
4.823	0.405	0.369	-0.036
5.448	0.485	0.470	-0.015
6.135	0.553	0.498	-0.055
6.76	0.612	0.575	-0.037
Reg. 19: P=7.2, N=308, G=1.76, T=539			
0.385	0	0	0
0.948	0.007	0	-0.007
1.573	0	0	0
2.322	0.05	0	-0.050
2.947	0.017	0	-0.017
4.01	0.124	0	-0.124
4.823	0.235	0.104	-0.132
5.448	0.31	0.199	-0.111
6.135	0.395	0.298	-0.097
6.76	0.465	0.381	-0.084
Reg. 20: P=7.2, N=524, G=0.44, T=460			
0.385	0	0	0
0.948	0	0	0
1.573	0	0	0
2.322	0.077	0.067	-0.010
2.947	0.34	0.295	-0.045
4.01	0.631	0.614	-0.017
4.823	0.841	0.741	-0.100
5.448	0.799	0.802	0.003
6.135	0.846	0.850	0.004
6.76	0.882	0.890	0.008
Reg. 21: P=7.2, N=515, G=0.88, T=461			
0.385	0.008	0	-0.008
0.948	0.002	0	-0.002
1.573	0	0	0
2.322	0	0	0
2.947	0	0	0
4.01	0	0	0
4.823	0.046	0	-0.046
5.448	0.144	0.092	-0.052
6.135	0.286	0.328	0.042
6.76	0.458	0.482	0.024
Reg. 22: P=7.3, N=513, G=0.88, T=514			
0.385	0.001	0	-0.001

	v		
	Exp	Calc	Δ
0.948	0.018	0	-0.018
1.533	0.015	0	-0.015
2.352	0.085	0.005	-0.080
2.947	0.22	0.192	-0.028
4.01	0.446	0.480	0.034
4.823	0.579	0.571	-0.008
5.448	0.654	0.643	-0.011
6.135	0.733	0.702	-0.031
6.76	0.79	0.765	-0.025
Reg. 23: P=7.2, N=516, G=1.32, T=485			
0.385	0.012	0	-0.012
0.948	0.012	0	-0.012
1.573	0.006	0	-0.006
2.322	0	0	0
2.947	0	0	0
4.01	0	0	0
4.823	0.041	0	-0.041
5.448	0.011	0	-0.011
6.135	0.059	0.023	-0.036
6.76	0.198	0.179	-0.019
Reg. 24: P=7.2, N=520, G=1.77, T=528			
0.385	0.021	0	-0.021
0.948	0.008	0	-0.008
1.573	0.004	0	-0.004
2.322	0.002	0	-0.002
2.947	0.066	0	-0.066
4.01	0.278	0.103	-0.175
4.823	0.435	0.281	-0.154
5.448	0.484	0.397	-0.087
6.135	0.468	0.483	0.015
6.76	0.534	0.558	0.024
Reg. 25: P=7.2, N=632, G=0.88, T=454			
0.385	0	0	0
0.948	0.004	0	-0.004
1.573	0.003	0	-0.003
2.322	0	0	0
2.947	0	0	0
4.01	0.065	0	-0.065
4.823	0.197	0.155	-0.042
5.448	0.332	0.402	0.070
6.145	0.511	0.518	0.007
6.76	0.65	0.640	-0.010

Average boundary conditions for each Regime (Reg.): P: outlet pressure [MPa], N: power [kW], G: mass flow rate [kg/s], T: inlet temperature [K]. Results: v: void fraction [-] at elevation Z [m].